Carbon 199 (2022) 132–140

Contents lists available at ScienceDirect

Carbon

journal homepage: www.elsevier.com/locate/carbon

Effect of tribologically-induced changes in surface termination of silicon-containing diamond-like carbon coatings on the resistance to biomolecule adsorption

Zixuan Li [a,b], Jennings Z. Ye [c], Jieming Yan [a,b], Nicolás Molina [a,b], Hsu-Ming Lien [a,b], Robert Chrostowksi [a,b], Cherno Jaye [d], Daniel A. Fischer [d], Jianliang Lin [e], Filippo Mangolini [a,c,*]

[a] Texas Materials Institute, The University of Texas at Austin, Austin, TX, 78712, USA
[b] Materials Science and Engineering Program, The University of Texas at Austin, Austin, TX, 78712, USA
[c] Walker Department of Mechanical Engineering, The University of Texas at Austin, Austin, TX, 78712, USA
[d] Materials Measurement Science Division, Material Measurement Laboratory, National Institute of Standards and Technology, Gaithersburg, MD, 20899, USA
[e] Southwest Research Institute, San Antonio, TX, 78238, USA

ARTICLE INFO

Keywords:
DLC
NEXAFS
Amorphous carbon
ATP

ABSTRACT

Silicon-containing diamond-like carbon (DLC) is a class of thin-film materials with excellent mechanical properties, high thermal stability, and good tribological performance over a wide range of environmental conditions. While non-alloyed/non-doped DLCs also exhibit good biocompatibility and bioinertness, our understanding of the effect of silicon in DLCs on biomolecules/DLC interactions is still elusive. Here, we evaluated the structural, mechanical, and tribological properties of Si-containing DLC coatings with silicon content fraction of 11% and 16%. Tribological tests, performed by sliding a stainless steel pin on the coatings in water, indicated a low friction response (steady-state coefficient of friction <0.11), while quartz crystal microbalance experiments indicated no adsorption of a model biomolecule, namely adenosine triphosphate (ATP), on Si-containing DLCs. Near-edge X-ray absorption fine structure spectromicroscopy analyses performed after tribological experiments provided evidence for an increase in the fraction of silanol surface terminal groups formed in the worn region upon sliding in water without any significant sp^3-to-sp^2 rehybridization of carbon atoms. The fraction of surface hydroxyl groups in the worn region increases with the silicon content in Si-containing DLC, which leads to a decrease in friction. This tribologically-induced change in surface termination did not lead to the adsorption of ATP upon incubation of tribotested samples in ATP solutions for several hours. These findings open the path for the use of Si-containing DLC in applications requiring good tribological properties in aqueous solution and an excellent resistance to biomolecule surface adsorption that is maintained even after tribologically-induced variations in surface termination.

1. Introduction

The long-term and safe use of medical devices (*e.g.*, knee or hip joints, heart valves, coronary stents) hinges on the development and use of materials and surface engineering solutions compatible with human cells, exhibiting good corrosion resistance, and having suitable load-carrying capabilities. Despite the widespread use of metallic implants, their surface degradation resulting from corrosion and/or wear brought safety concerns related to their use into focus as the release in the human body of wear debris and metallic ions can lead to pseudo-tumor formation [1], osteolysis, and, potentially, implant failure [2]. Among the solutions proposed so far to alleviate or even prevent these problems and increase the lifetime of implants, diamond-like carbon (DLC) films have extensively been considered given their excellent mechanical properties (*i.e.*, high stiffness and hardness) [3], good tribological behavior (*i.e.*, high wear resistance and low friction) [4], chemical inertness, as well as good biocompatibility and bioinertness [2,5–20]. As a particular example, DLC films exhibited good hemocompatibility, which results in a reduction of cytotoxic reactions and thrombosis formation [2,7,16]. Allen et al. demonstrated that DLC coatings do not cause cytotoxicity *in vitro* as cells derived from the tissues surrounding a total joint replacement (*i.e.*, macrophages, osteoblast-like cells, and fibroblasts) exhibited

* Corresponding author. Texas Materials Institute, The University of Texas at Austin, Austin, TX, 78712, USA.
E-mail address: filippo.mangolini@austin.utexas.edu (F. Mangolini).

https://doi.org/10.1016/j.carbon.2022.07.043
Received 4 April 2022; Received in revised form 24 May 2022; Accepted 17 July 2022
Available online 1 August 2022

normal growth and morphology on DLCs [19]. Linder et al. provided evidence for the biocompatibility of DLC-coated surfaces as both cytoskeletal activation status and architecture of primary macrophages were not influenced by their formation on DLCs [16].

Despite the relevance of these studies, some limitations have emerged and currently hinder the use of DLC films for creating biocompatible surfaces for medical devices. In the case of DLC coatings containing significant amounts of hydrogen (hydrogen content fraction up to 40% [21,22]), which include a large fraction of sp^2-bonded carbon and have a low residual stress level, the relatively low hardness and Young's modulus [22] can negatively affect their long-term wear resistance when used in medical implants. For example, Fontaine et al. measured hardness values of 13 GPa and 11 GPa [23] for DLC coatings with a hydrogen content fraction of, respectively, 34% and 40% and a fraction of sp^2-bonded carbon of, respectively, 0.51 and 0.41 [24].

The introduction of dopants and alloying elements has been demonstrated to be an effective solution to improve the properties of DLC coatings [25]. Among the different types of alloyed and doped DLC materials developed so far, those containing silicon (with or without oxygen) have extensively been evaluated given their enhanced stability at elevated temperatures [26,27], reduced residual stress (<1 GPa) [28], and excellent tribological response under different environmental conditions [28–31]. Recently, Mangolini et al. and Hilbert et al. provided evidence that silicon- and oxygen-containing DLC coatings ([Si] = 6% ± 1%; [O] = 3% ± 1%; [H] = 34% ± 1%) have higher thermal stability than unalloyed DLCs due to the presence of silicon-carbon bonds, whose longer bond length relative to carbon-carbon sp^3 bonds results in a lower fraction of strained carbon-carbon bonds that can easily break at elevated temperature [32,33]. The generation of a silica-rich surface layer upon annealing under aerobic conditions was also shown by the authors to create an oxygen diffusion barrier that prevents the volatilization of the underlying carbon-rich film, thus drastically decreasing the erosion rate of silicon- and oxygen-containing DLC coatings compared to unalloyed DLCs [26,27].

Concerning the tribological response of Si-containing DLCs, Gilmore and Hauert showed that the introduction of ≈4% of silicon in DLC films results in a friction response that is less dependent on environmental conditions (*i.e.*, relative humidity) when sliding against steel [34]. Additionally, while undoped hydrogenated DLC exhibit very high specific wear rate in aqueous solutions, the introduction of silicon in hydrogenated DLCs was reported to significantly increase the wear resistance of the coatings [35,36]. Recently, Mangolini et al. performed tribological experiments using a silicon- and oxygen-containing DLC sliding against steel as a function of hydrogen and oxygen partial pressure and provided evidence that the tribological response of the coating under consideration is dependent on its gas pressure-dependent surface termination [30]. In addition to changes in surface termination, a significant rehybridization of carbon atoms from sp^3-to sp^2-bonding occurred in the near-surface region upon sliding. In the case of tribological tests carried out in the presence of water molecules, the detection of silanol groups (Si–OH) on the surface of Si-DLC films was proposed to originate from the dissociative adsorption of water and generate a water-rich layer able to reduce friction [37]. Since *ab initio* molecular dynamics simulations revealed that hydroxyl groups also passivate diamond surfaces as a result of the dissociative adsorption of water molecules confined between diamond films in relative motion [38], Kajita and Righi recently performed first-principles density functional theory calculations to investigate the effect of silicon dopants on water adsorption on diamond [39]. The results indicated that silicon dopants largely decrease (by more than 50%) the energy barrier for water dissociation on diamond surfaces. Notably, this surface hydroxylation of diamond (either with or without silicon dopants) enhances the attraction of further water molecules by forming a hydrogen bond network.

While these studies have provided insights into the effect of alloying elements on the structure of DLC films and the resulting mechanical and physicochemical properties, remarkably little is known about the biocompatibility of Si-containing DLCs. Ahmed et al. evaluated the adsorption of amino acid glycine on silicon-doped DLC with systematically varied silicon concentration (from 6% to 13%. Note: the film composition was obtained from X-ray photoelectron spectroscopy (XPS) analyses, *i.e.*, without accounting for the hydrogen content in the films) [40] and demonstrated that the amount of surface-adsorbed glycine decreases with the silicon content in the films. Despite the relevance of this study, our understanding of the evolution of the surface termination of alloyed DLCs upon sliding in aqueous solutions and its effect on the surface adsorption of biomolecules is still elusive. The present work aims to fill this knowledge gap by depositing DLC films with different concentration of silicon and performing tribological experiments in aqueous solutions. The analysis of the coatings by *ex situ* near-edge X-ray absorption fine structure (NEXAFS) spectromicroscopy not only allowed for determining the surface chemical changes occurring on Si-containing DLCs upon sliding in aqueous solutions, but also enabled the evaluation of the effect of changes in surface chemistry on the adsorption of a model biomolecule, namely adenosine triphosphate (ATP).

2. Experimental

2.1. Deposition of Si-containing DLC coatings

The deposition of Si-containing DLC coatings was carried out in a cubic meter vacuum chamber. The chamber has two rectangular-shaped magnetrons installed vertically and facing one another. The substrate material was made of ASTM 316L steel. The substrates, which were respectively cleaned in acetone and alcohol before being loaded into the chamber, were hanging down from a planetary double rotation fixture. Fig. 1 presents a schematic drawing of the deposition system. The chamber was baked at 250 °C until a base pressure less than 4×10^{-5} Pa was achieved. After reaching high vacuum, the substrates were firstly cleaned by an Argon-discharged plasma at −650 V using pulsed dc. After

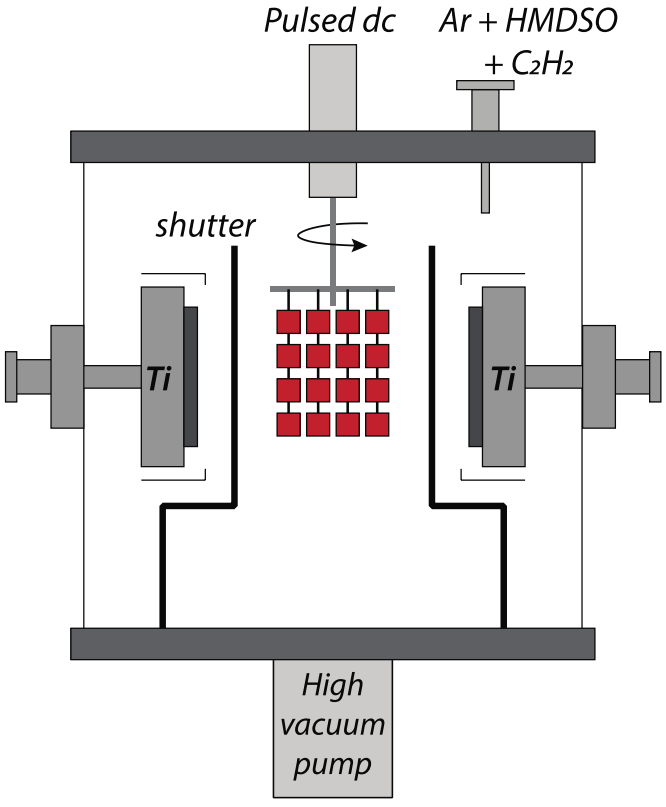

Fig. 1. Schematic drawing of the deposition system used for growing Si-containing DLC coatings. (A colour version of this figure can be viewed online.)

substrate cleaning, a thin titanium bond layer was deposited by sputtering a pure titanium target in Argon using DC (Advanced Energy Pinnacle).

After the titanium bond layer was deposited, the titanium target power was turned off and the chamber was backfilled with a gas mixture of Argon, hexamethyldisiloxane (HMDSO), and acetylene (C_2H_2). A pulsed voltage (Advanced Energy Pinnacle plus) was applied to the substrates to generate a glow discharge plasma for the deposition of DLC films. In this study, two Si-containing DLC coatings were deposited at different HMDSO and C_2H_2 flow rates. Table 1 summarizes the key deposition parameters for the coatings.

2.2. Methods

Tribological experiments were carried out using a Bruker UMT TriboLab (Bruker, USA). Reciprocating ball-on-discs tests (normal load: 10 N, stroke length: 4 mm, sliding speed: 2 mm/s. Average Hertzian contact pressure: 1.0 GPa) were performed in the boundary-lubrication regime using ASTM 316L steel substrates coated with Si-containing DLC and ASTM 304 steel counterparts (diameter: 4 mm). All experiments were carried out in air (relative humidity: 37% ± 5%) and at room temperature (23 °C ± 2 °C). The tribological contact was immersed in ultrapure Milli-Q water (electrical conductivity: 18.2 MΩ cm). After the tribological tests (test duration: ~200 s), the samples were dried under a nitrogen (N5) stream.

The surface chemistry of the Si-containing DLC coatings was characterized by X-ray photoelectron spectroscopy (XPS). XPS analyses were carried out using a Kratos Axis Ultra DLD XPS (Kratos Analytical Ltd, UK), which was equipped with a monochromatized Al Kα X-ray source and calibrated according to ISO 15472:2001 (accuracy: ±0.1 eV). The base pressure in the XPS analysis chamber was always $<1 \times 10^{-6}$ Pa. In this work, XPS data were acquired in constant-analyzer-energy mode with an X-ray beam diameter of 200 μm and a photoelectron emission angle of 0°. Survey XPS spectra were collected with a pass energy of 160 eV, while high-resolution XPS spectra were acquired with a pass energy of 40 eV (corresponding to a full-width-at-half-maximum of Ag $3d_{5/2}$ of 0.77 eV). Data processing was performed using CasaXPS (v2.3.23, Casa Software Ltd, UK) and included background subtraction, which was carried out using an iterated Shirley-Sherwood algorithm, prior to peak fitting. The quantification of the surface composition was performed employing the method described in Refs. [41,42]. Briefly, once the integrated intensity (*i.e.*, the peak area) was determined, the surface composition was quantified using the first-principles method [43]. The inelastic mean free path was calculated using the Gries G1 formula [44].

Rutherford backscattering spectrometry (RBS) with hydrogen forward scattering (HFS) measurements were performed by Evans Analytical Group (USA). RBS spectra were acquired using a 2.275 MeV He^{2+} ion beam with normal and grazing detector angles of, respectively, 160° and ≈100° (the sample is perpendicular to the incident He^{2+} ion beam). For HFS measurements, the grazing detector angle was placed 30° from the forward trajectory of the incident He^{2+} ion beam and the sample was rotated to have the He^{2+} ion beam impinging the surface with an angle of 75° relative to the surface normal.

Raman measurements were carried out using a confocal Raman imaging system (Witec alpha300 R, Witec, Germany) equipped with two lasers having wavelength of 488 nm and 532 nm. In this work, Raman spectra were acquired on several points to check for surface heterogeneity and with a laser power <100 μW to avoid any damage. Peak fitting was carried out after linear background subtraction using Gaussian synthetic curves (IgorPro V.9 software, WaveMetrics Inc., USA).

Nanoindentation measurements were performed with an Hysitron Triboindenter TI 950 (Hysitron, Bruker, USA) in depth-controlled indentation mode. All experiments were performed at room temperature and in air. Before each set of experiments, the shape of the Berkovich diamond indenter was determined from nanoindentation experiments performed on fused silica.

Quartz crystal microbalance (QCM) experiments were carried out using a QSense Explorer QCM (Biolin Scientific, Sweden). The stainless steel (SS) crystals were cleaned in sodium dodecyl sulfate (20% in DI water) for 20 min and subsequently rinsed with DI water. Before being mounted in the QCM flow cell, the SS crystals were sonicated in ethanol for 10 min and UV-O_3 cleaned for 10 min. As for the Si-containing DLC-coated crystals, they were sonicated in ethanol for 20 min before use. All QCM experiments were carried out at room temperature using a flow rate of 50 μL/s. Adenosine triphosphate (ATP, Sigma Aldrich) aqueous solution (ATP concentration: 300 mg/L) was freshly prepared before being used for the QCM experiments presented in this work.

Near-edge X-ray absorption fine structure (NEXAFS) spectromicroscopy measurements were carried out at beamline 7-ID-1 (SST-1) at the National Synchrotron Light Source II (NSLS-II, Brookhaven National Laboratory, USA). The endstation includes a commercial full-field spectromicroscope extensively described in Refs. [45,46] and known as the Large Area Rapid Imaging Analytical Tool (LARIAT, Synchrotron Research Inc., Melbourne Beach, FL, USA). It enables X-ray absorption analyses to be performed with a 13 mm × 18 mm field of view and a lateral resolution of ≈50 μm. NEXAFS data were collected in partial electron yield (PEY) mode at a photon energy between 130 eV and 145 eV (phosphorus L-edge), 270 eV and 330 eV (carbon K-edge), 380 eV and 430 eV (nitrogen K-edge), and 520 eV and 570 eV (oxygen K-edge). The photon energy resolution was 0.1 eV. Data processing was performed using LDF software (Synchrotron Research Inc., Melbourne Beach, FL, USA) and included the normalization of NEXAFS images to the drain current that was simultaneously measured from a clean Au-coated mirror upstream of the endstation. NEXAFS images were subsequently normalized by the pre-edge intensity. A post-edge intensity normalization was also applied to NEXAFS data acquired at the C K-edge and O K-edge so that any variation in spectral intensity is independent of the number density of absorbing atoms and only due to changes in bonding environment.

The fraction of sp^2-hybridized carbon (f_{sp^2}) was quantified from NEXAFS spectra using the procedure outlined in Refs. [47,48]. Briefly, the methodology employs the relative area of the C 1s→π* and C 1s→σ* signals for the sample under investigation and a reference sample:

$$f_{sp^2} = \frac{I^{\pi^*}_{sample}}{I_{sample}(\Delta E)} \frac{I_{ref}(\Delta E)}{I^{\pi^*}_{ref}} \quad \text{Eq. 1}$$

where $I^{\pi^*}_{sample}$ and $I^{\pi^*}_{ref}$ are the areas of the C 1s→π* peaks for, respectively, the sample and the reference, while $I_{sample}(\Delta E)$ and $I_{ref}(\Delta E)$ are the integrated spectral intensity between 288.6 eV and 320 eV for, respectively, the sample and the reference. Reference C K-edge NEXAFS spectra were acquired on freshly-cleaved highly ordered pyrolytic graphite (HOPG, grade 2, SPI Supplies, West Chester, PA, USA) (100% sp^2-bonded carbon) using the procedure outlined in Refs. [47–49].

The uncertainties reported in the present work were computed from three independent measurements.

Table 1
Deposition parameters for the DLC coatings.

	Ar (sccm)	HMDSO (g/min)	C_2H_2 (sccm)	Substrate voltage (V)	Chamber pressure (Pa)
"Low" Si-containing DLC	20	5	200	−650	0.27
"High" Si-containing DLC	20	6	120	−650	0.16

3. Results & discussion

As-deposited, Si-containing DLC coatings were first analyzed to determine their structure, mechanical properties, and composition. Survey XPS spectra (Figure S.1 in the Supporting Information) showed the presence of the characteristic photoelectron signals of carbon (C 1s at 285 eV), oxygen (O 1s at 530 eV), and silicon (Si 2p at 100 eV and Si 2s at 151 eV) [50]. The high-resolution C 1s spectra (Fig. 2a) were fit with five components at (283.3 ± 0.1) eV (assigned to carbon bonded to silicon as in silicon carbide [50,51]), (284.4 ± 0.1) eV (assigned to carbon-carbon and carbon-hydrogen bonds in DLC [52] and silicon- and oxygen-containing DLC [32] as well as to carbon bonded to silicon in organosiloxanes [53–55]), (285.0 ± 0.1) eV (assigned to aliphatic carbon contamination [50,53]), and (286.4 ± 0.1) eV and (287.8 ± 0.1) eV (assigned to carbon bonded to oxygen deriving from the sample exposure to air [53,56]). The O 1s spectra (Fig. 2b) turned out to contain three peaks, which were assigned to oxygen bonded to silicon [53] (at 532.1 eV ± 0.2 eV. This peak includes a small contribution from carbonyl oxygen [53]), oxygen bonded to carbon [53] (at 533.1 eV ± 0.2 eV) and surface-adsorbed water (at 534.1eV ± 0.2 eV). Since the Si 2p spectra (Fig. 2c) is the convolution of the $2p_{1/2}$ and $2p_{3/2}$ signals due to spin-orbit coupling, curve synthesis was carried out using two synthetic curves with area ratio equal to 2 and energy separation equal to 0.65 eV. The maxima of the Si $2p_{3/2}$ components were found at (100.6 ± 0.2) eV (assigned to Si(I) and Si bonded to C as in silicon carbide [32, 51,57–59]), (101.4 ± 0.2) eV (assigned to Si(II) [32,51,57–59]), (102.2 ± 0.2) eV (assigned to Si(III) [32,51,57–59]), and (103.5 ± 0.2) eV (assigned to Si(IV) [32,51,57–59]). Notably, the distribution of the different silicon oxidation states was not significantly different in the two as-deposited coatings. The fractional composition of the near-surface region, calculated on the basis of XPS data, was found to be [C] = (72 ± 1) %, [O] = (12 ± 1) %, and [Si]= (15 ± 1) % for Si-containing DLC grown in the presence of both HMDSO (5 g/min) and C_2H_2 (200 sccm), while it was calculated to be [C] = (59 ± 1) %, [O] = (17 ± 1) %, and [Si] = (23 ± 1) % for Si-containing DLC grown in the presence of HMDSO (6 g/min) and C_2H_2 (120 sccm). Because of the different silicon content, in the following these two coatings will be referred to as "low Si-containing DLC" and "high Si-containing DLC", respectively.

As XPS does not allow for the determination of the hydrogen content [60], RBS/HFS depth-profile measurements (Fig. 3a and b) were carried out and enabled the bulk fractional composition of the as-grown coatings to be determined (Fig. 3c) ([C] = (65 ± 4) %, [O] = (5 ± 3) %, [Si] = (11 ± 1) %, [H] = (19 ± 2) % for the "low" Si-containing DLC grown in the presence of both HMDSO (5 g/min) and C_2H_2 (200 sccm); [C] = (58 ± 4) %, [O] = (7 ± 3) %, [Si] = (16 ± 1) %, [H] = (19 ± 2) % for the "high" Si-containing DLC grown in the presence of HMDSO (6 g/min) and C_2H_2 (120 sccm)). Notably, the comparison of the RBS/HFS results with the outcomes of quantitative XPS analyses (surface sensitive. The information depth computed using the Gries G1 formula [44] is 9.5 nm) indicated a good agreement between the [C]/[Si], but a slightly lower [O]/[Si] value for the RBS/HFS data, thus suggesting the presence, in the as-deposited films, of a slightly surface-oxidized layer.

To gain insights into the structure of the as-deposited Si-containing DLC coatings, multi-wavelength Raman spectroscopic analyses were carried out (Fig. 4). As the scattering cross-section of π states is much higher (more than 50x [3]) than the scattering cross-section of σ states, the visible Raman spectra of DLC materials are characterized by a broad envelope that includes a signal near 1513 cm^{-1} (the so-called G band) corresponding to the in-plane bond stretching of pairs of sp^2 carbon atoms (either in chains or rings) and a signal near 1297 cm^{-1} (the so-called D band) corresponding to the breathing mode of sp^2 carbon atoms in sixfold aromatic rings [61]. Compared to the Raman spectra acquired at 532 nm on "low" Si-containing DLC, the ones acquired at 532 nm on "high" Si-containing DLC exhibited a lower ratio of the integrated intensity of the D and G bands (*i.e.*, I_D/I_G. I_D/I_G = 0.51 ± 0.05 for "high" Si-containing DLC and I_D/I_G = 0.74 ± 0.07 for "low" Si-containing DLC), which suggests a decrease in the size of sp^2 ring-like carbon cluster [61–63]. Following the methodology described by Rose et al. [64] and Cui et al. [65], the fraction of sp^2-bonded carbon could be quantified from the dispersion of the G band and found to be 0.44 ± 0.06 and 0.38 ± 0.06 for, respectively, the "low" and "high" Si-containing DLC coatings. The increase in the fraction of sp^3-bonded carbon with the Si content is in good agreement with experimental results obtained from DLC films with different [Si] [66–69].

Fig. 5a and c respectively display the evolution of the reduced elastic modulus (E^*) and hardness (H) as a function of depth from the sample surface obtained from nanoindentation data. The average values of E^* and H computed considering an indentation depth between 50 nm and 90 nm (<10% of the coating thickness) are respectively reported in Fig. 5b and d. The elastic moduli computed assuming a Poisson's ratio of 0.2 for Si-containing DLC, an elastic modulus for the indenter of 1141 GPa, and a Poisson's ratio of 0.07 for the indenter [70] were (202 ± 12) GPa and (171 ± 7) GPa for "low" and "high" Si-containing DLC coatings, respectively. The slight decrease in hardness and elastic modulus upon increasing the Si content in the film is in agreement with previous studies correlating the mechanical properties of Si-containing DLC (with [Si] < 20%) with the silicon concentration [68,71]. Notably, Ohtake et al. recently performed a systematic study of the dependence of the hardness of DLC on different structural parameters, including carbon

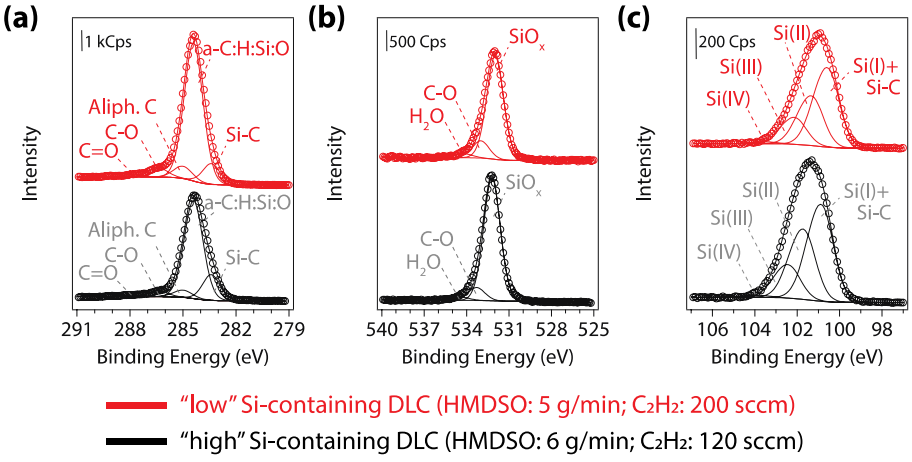

Fig. 2. High-resolution XPS spectra ((a): C 1s; (b) O 1s; (c) Si 2p) acquired on as-deposited "low" and "high" Si-containing DLC films. (A colour version of this figure can be viewed online.)

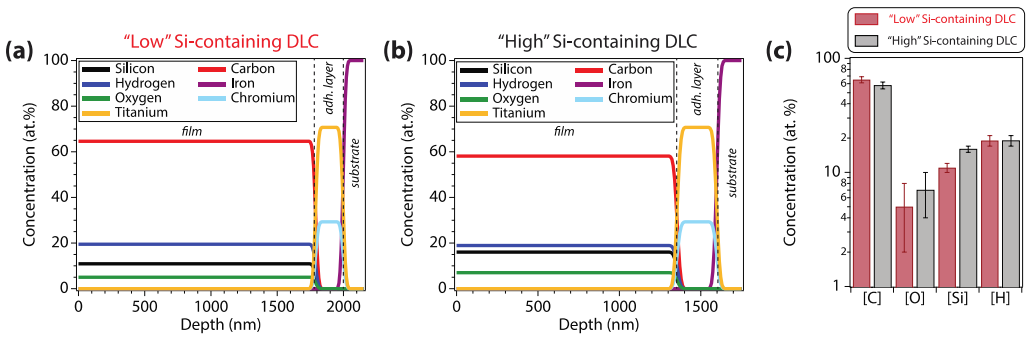

Fig. 3. Rutherford backscattering spectrometry with hydrogen forward scattering depth profile of (a) "low" Si-containing DLC and (b) "high" Si-containing DLC. (c) Average composition of the two coatings computed considering a depth between 250 nm and 1500 nm for "low" Si-containing DLC and between 250 nm and 1000 nm for "high" Si-containing DLC. (A colour version of this figure can be viewed online.)

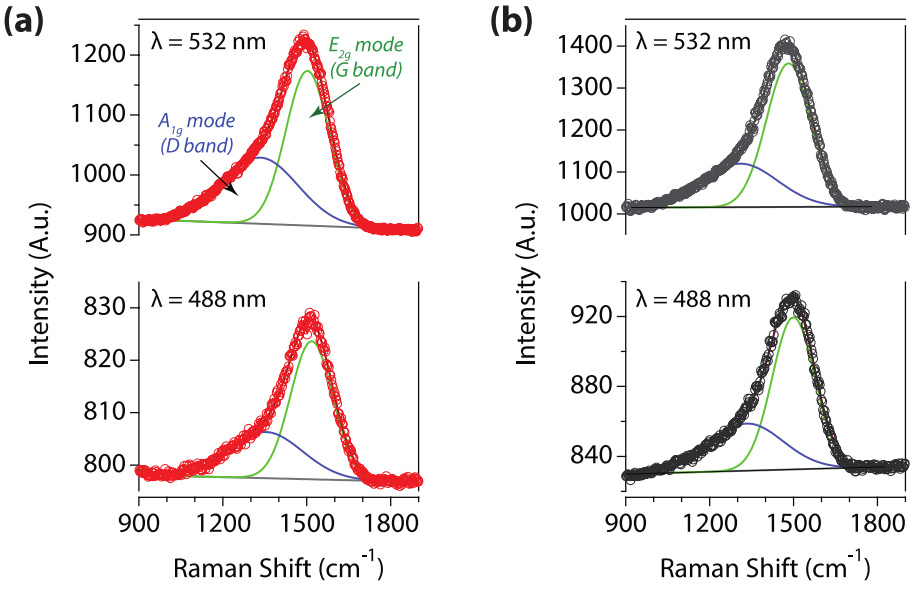

Fig. 4. Multi-wavelength Raman spectra (λ = 532 nm and λ = 488 nm) acquired on: (a) "low" Si-containing DLC films; and (b) "high" Si-containing DLC films. (A colour version of this figure can be viewed online.)

hybridization and hydrogen content [72]. The comparison of the hardness values (≈17–18 GPa) reported by Ohtake et al. for undoped DLC coatings grown plasma-enhanced chemical vapor deposition that have a hydrogen content (≈20 at.%) and a fraction of sp^2-bonded carbon (0.4) similar to the films evaluated in this study, indicate that the introduction of silicon in DLC slightly increases the mechanical properties.

Fig. 6a displays the typical QCM results obtained when evaluating the adsorption of ATP on stainless steel (SS) using an aqueous solution with ATP concentration of 300 mg/L. Upon injecting ATP in the QCM flow cell, a negative frequency shift occurs, indicating the adsorption of ATP molecules on the SS-coated crystal. The mass before the rinsing step represents the equilibrium mass of adsorbed ATP in the presence of excess ATP molecules in the solution, which implies that both physisorbed and chemisorbed molecules contribute to the frequency shift. Upon exchanging the ATP solution with pure DI water, the desorption of loosely bound ATP molecules occurs, as indicated by a positive frequency shift (*i.e.*, a decrease in adsorbed mass). The mass measured after the rinsing step is thus representative of the chemisorbed ATP molecules on stainless steel without any excess ATP in the solution.

In the case of the QCM experiments performed with Si-containing DLC-coated (with either "high" or "low" silicon content) crystals, no frequency shifts were observed after injecting ATP or during the rinsing step, thus indicating no measurable adsorption of ATP on these coatings. A typical single-injecting QCM measurement performed with a QCM crystal coated with Si-containing DLC is displayed in Fig. 6b. These results corroborate previous studies that provided evidence for the good biocompatibility and bioinertness of DLC coatings reported in the published literature [2,5–20].

To evaluate changes in surface termination of Si-containing DLCs upon sliding in the presence of water molecules and their effect on the surface adsorption of ATP, tribological experiments were performed by sliding an ASTM 304 steel pin on Si-containing DLC coatings in DI water for different number of cycles (*i.e.*, 1/2, 5, 25, and 50 cycles) (Fig. 7). The coefficient of friction (CoF) slowly decreased from ≈0.15 (for both coatings) with the number of sliding cycles and reached a plateau at 0.076 ± 0.006 after 20 cycles for the case of "high" Si-containing DLC, while a CoF of 0.102 ± 0.008 was reached by "low" Si-containing DLC only after 40 cycles.

To determine the surface phenomena occurring on Si-containing DLC upon sliding and affecting the friction response of Si-containing DLC, *ex situ* NEXAFS spectromicroscopy analyses were subsequently carried out. Fig. 8a displays a schematic of a Si-containing DLC sample on which multiple sliding experiments were performed for different number of cycles. The use of the rapid parallel processing magnetic field electron yield optics detector at the National Synchrotron Light Source II (NSLS-II, beamline 7-ID-1) allowed for the acquisition of two-dimensional NEXAFS image stacks, *i.e.*, NEXAFS maps collected as the photon energy is scanned across X-ray absorption edges of interests (carbon K-

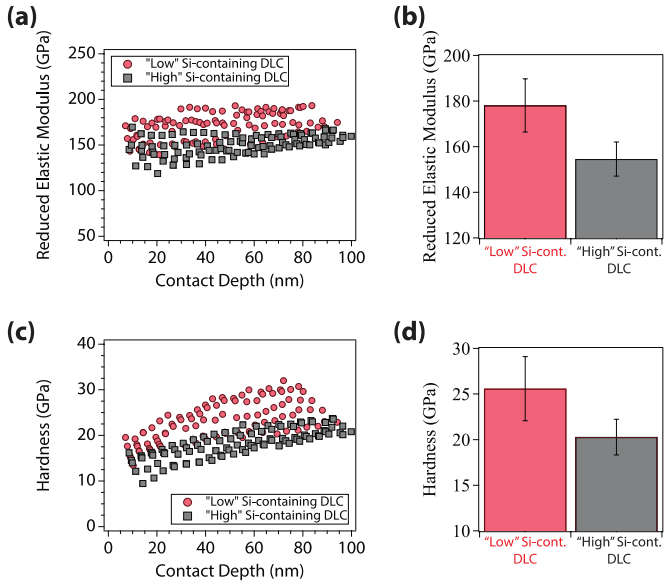

Fig. 5. (a) Reduced elastic modulus and (c) hardness for as-deposited "low" and "high" Si-containing DLC films as a function of indentation depth. The average reduced elastic moduli and hardness calculated for an indentation depth between 50 nm and 90 nm are, respectively, displayed in (b) and (d). (A colour version of this figure can be viewed online.)

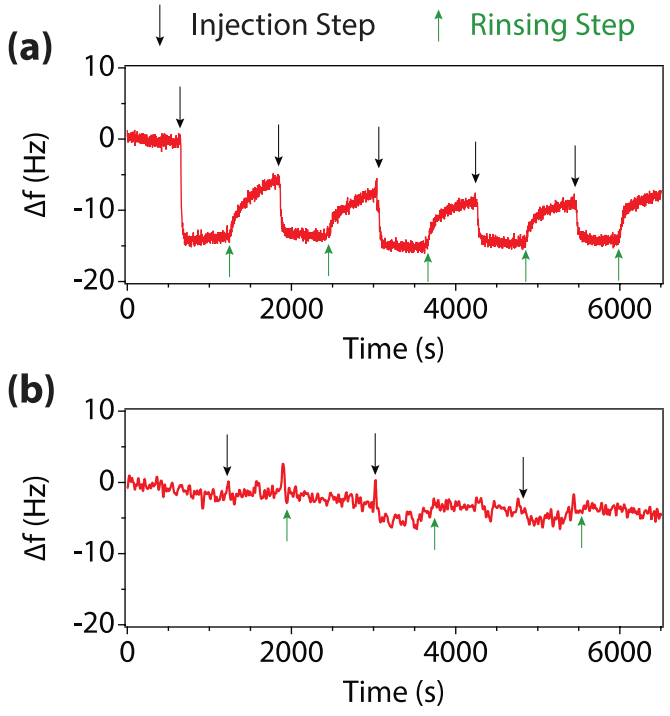

Fig. 6. Change in frequency (Δf) as a function of time for (a) a stainless steel-coated QCM crystal and (b) "high" Si-containing DLC-coated crystal. Similar results to the ones displayed in (b) were obtained when using "low" Si-containing DLC-coated crystals. (A colour version of this figure can be viewed online.)

edge, oxygen K-edge, nitrogen K-edge, and phosphorus K-edge). Fig. 8b displays an example of partial electron yield NEXAFS C K-edge map obtained by summing up the NEXAFS images collected with photon energy between 280 eV and 292 eV. The map of the sample (a "high" Si-containing DLC) allowed for locating the four wear tracks generated during tribological testing and extracting NEXAFS spectra from regions

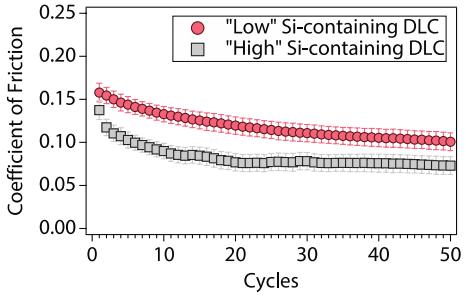

Fig. 7. Coefficient of friction as a function of sliding cycles obtained during reciprocating ball-on-discs tests carried out in water using ASTM 316L steel substrates coated with Si-containing DLC and ASTM 304 steel counterparts. (A colour version of this figure can be viewed online.)

of interest (ROIs), namely inside and outside the tracks. For both "low" and "high" Si-containing DLC samples, the C K-edge NEXAFS spectra extracted from the wear tracks did not exhibit any significant differences compared to the spectrum obtained from the non-contact region. Fig. 8c displays an example set of C K-edge spectra collected on a "high" Si-containing DLC specimen, while Fig. 8d displays a zoomed-in view of the absorption edge. A broad envelope was detected between 287 eV and 320 eV, which originates from the C 1s→σ* transition for carbon-carbon σ (disordered) bonds [49,73], while a well-defined feature was found at (284.9 ± 0.2) eV, which derives from the C 1s→π* transition for carbon-carbon (disordered) bonds [49,73]. The integrated intensity of the latter can be correlated with the fraction of sp^2-hybridized carbon in the probed volume [47,73–76]. Additional absorption features were detected at (287.0 ± 0.2) eV, which was assigned to the C 1s→σ* transition for C–H bonds [49,75,76], and at (288.9 ± 0.2) eV (assigned to the C1s→σ* transitions for carbon-silicon and carbon-oxygen bonds [77,78]). The presence of carbonyl groups in the near-surface region of the coatings could also contribute to the intensity between 286.5 eV and 287.0 eV (C1s→π* transition of C═O) [49,79]. The acquisition of NEXAFS C K-edge spectra allowed for the determination of the fraction of sp^2-bonded carbon in Si-containing DLCs: the values computed from the non-contact regions (*i.e.*, 0.48 ± 0.03 for "low" Si-containing DLC and 0.42 ± 0.03 for "high" Si-containing DLC) agree well with those calculated from multiwavelength Raman measurements performed on the as-deposited specimens. Notably, no significant differences in the fraction of sp^2-hybridized carbon were observed inside the wear tracks, thus indicating that no stress-assisted rehybridization of carbon atoms from sp^3 to sp^2 bonding occurred during the sliding process.

The O K-edge (pre- and post-edge normalized) spectra acquired on "low" and "high" Si-containing DLC samples are displayed in Fig. 8e and f, respectively. The spectra exhibit a small pre-edge absorption peak at (532.6 ± 0.2) eV together with a broad envelope at (529–540) eV. The former can be ascribed to the presence of surface O–H groups together with C═O groups (O1s→π* transition of C═O [80,81]), while the latter is due to O1s→σ* transition of oxygen bonded to silicon and carbon [82,83]. Upon sliding in DI water, a significant and progressive increase in intensity for the peak detected at low photon energies (≈532.6 eV) was observed. Since no significant changes were detected in the C K-edge spectra extracted from the wear tracks compared to the spectrum of the unworn region (in particular, the intensity of the absorption features assigned to carbon bonded to oxygen did not significantly vary), the increase in intensity of the pre-edge peak in the O K-edge spectra could be assigned to the formation of silanol groups (Si–OH). The finding provides experimental evidence corroborating first-principles calculations performed by Kajita and Righi [39], which indicated that doping diamond with silicon reduces the energy barrier for water dissociation on diamond by stabilizing the hydroxylated configuration and resulting in the generation of surface silanol groups that attract further water molecules. The comparison of the O K-edge spectromicroscopy data

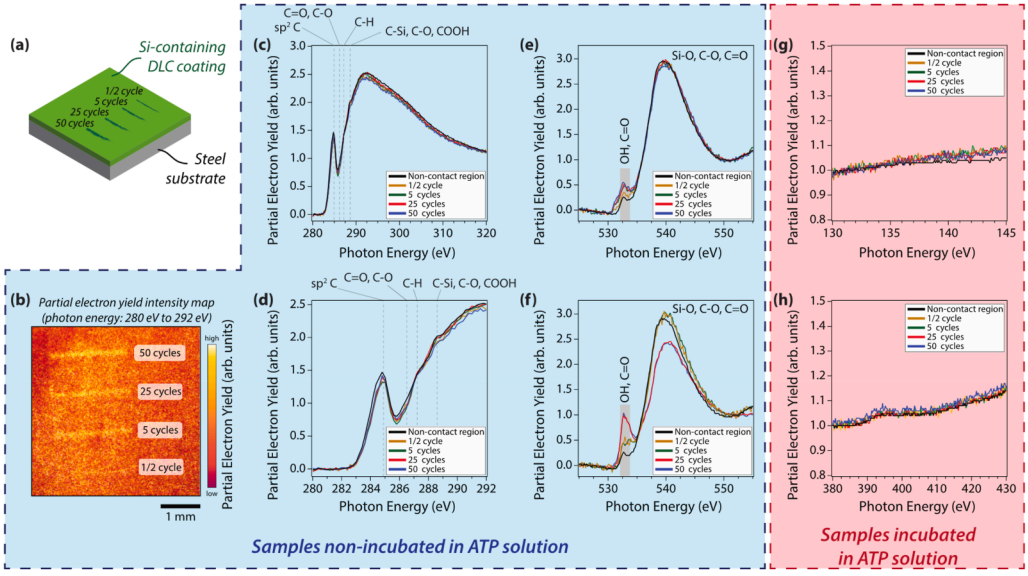

Fig. 8. (a) Schematic of the tribological experiments performed on Si-containing DLC; (b) partial electron yield NEXAFS map collected on a "high" Si-containing DLC on which four tribological tests were carried out for different number of cycles; (c) carbon K-edge NEXAFS spectra of "high" Si-containing DLC extracted from the non-contact and contact regions of the carbon K-edge NEXAFS map; (d) zoomed-in view of the carbon K-edge NEXAFS spectra of "high" Si-containing DLC shown in (c); (e) oxygen K-edge NEXAFS spectra of "low" Si-containing DLC extracted from the non-contact and contact regions of the oxygen K-edge NEXAFS map; (f) oxygen K-edge NEXAFS spectra of "high" Si-containing DLC extracted from the non-contact and contact regions of the oxygen K-edge NEXAFS map; (g) phosphorus L-edge and (h) nitrogen K-edge NEXAFS spectra of "high" Si-containing DLC extracted from the non-contact and contact regions of the carbon K-edge NEXAFS maps. The nitrogen K-edge and phosphorus L-edge NEXAFS maps were obtained after incubating tribologically-stressed samples in a 300 mg/L ATP aqueous solution for 11 h. (A colour version of this figure can be viewed online.)

acquired on "low" and "high" Si-containing DLC also suggested that increasing the silicon content in the coating results in an increase in the hydroxyl surface terminal groups created upon sliding in water, as a much larger increase in the intensity of the pre-edge absorption peak assigned to O–H bonds was detected in the case of "high" Si-containing DLC (Fig. 8e and f). Finally, the analysis of the O K-edge NEXAFS spectra that were only pre-edge normalized (Figure S.2 in the Supporting Information) could be used to highlight differences in the concentration of oxygen in the near-surface region as the intensity in the post-edge region (≈550 eV in the case of the O K-edge) is proportional to the number density of absorbing atoms [49]: while in the case of the spectra acquired on "low" Si-containing DLC no significant changes in the intensity of the post-edge region were observed, in the case of the data collected on "high" Si-containing DLC the post-edge (≈550 eV) intensity progressively increased with the number of sliding cycles, which indicates a substantial increase in the concentration of oxygen atoms in the wear tracks, especially in those created upon sliding for several cycles. Altogether, the O K-edge spectra suggest that increasing the silicon content in Si-containing DLCs stabilizes a hydroxylated surface configuration. This is proposed to be the origin for the lower friction response of "high" Si-containing DLC compared to the one of "low" Si-containing DLC.

Altogether, the NEXAFS spectromicroscopy results provided new insights into the origin of the low friction response of Si-containing DLCs in aqueous solutions as they demonstrate that the stress-induced formation of a surface layer that is rich in sp^2-bonded carbon is not a sufficient condition for reaching a low friction response and that the formation of silanol functional groups as a result of the dissociative reaction of water molecules is critical for decreasing the shear strength of the sliding interface.

To evaluate the effect of changes in surface termination (without any variation in the carbon rehybridization state, as indicated by the C K-edge NEXAFS data) on the adsorption of ATP on Si-containing DLCs, the samples were incubated in a 300 mg/L aqueous solution for 11 h immediately after tribological testing. NEXAFS spectromicroscopy measurements enabled the extraction of P L-edge and N K-edge spectra from the worn and unworn regions. No absorption signals were detected in either the P L-edge and N K-edge spectra acquired on both "low" and "high" Si-containing DLC. An example of these spectra is displayed in Fig. 8g and h for the case of a "high" Si-containing DLC. This finding demonstrates that, despite the increase in the fraction of silanol surface terminal groups that might promote the surface adsorption of molecules via hydrogen bonding, no significant adsorption of ATP occurred on Si-containing DLC surfaces. We propose that the lack of adsorption of ATP inside the wear tracks at pH 7 is due to the long-range electrostatic repulsive interactions occurring between negatively charged ATP molecules and the negative charge that develops on the Si-containing DLC surface as a result of the deprotonation of silanol terminal groups at pH 7. Previous studies, in fact, have provided evidence that at environmentally relevant pH values (*i.e.*, between 5 and 8) the phosphate groups in nucleotides (*e.g.*, ATP) are deprotonated [84,85] and the isoelectric point of silica containing silanol groups is at pH ~3 [84–86].

While the results reported here were obtained with a model biomolecule, *i.e.*, ATP, the experimental framework can be extended to other biomolecules, thus opening the path for the systematic evaluation of the biocompatibility of Si-containing DLCs and its potential application in biomedical devices.

4. Conclusions

In summary, Si-containing DLC coatings with varied composition (silicon content of 11% and 16%) were grown on steel and characterized by XPS, Raman, and NEXAFS spectroscopy as well as RBS/HFS spectrometry and nanoindentation. The good mechanical properties of the coatings (hardness >20 GPa; elastic modulus >170 GPa) combine with a low friction response in water while sliding against a stainless steel pin. QCM experiments indicated that, in contrast to stainless steel, negligible adsorption of a model biomolecule (*i.e.*, ATP) occurred on Si-containing DLCs. Surface-analytical measurements performed after tribological experiments provided evidence for an increase in the fraction of silanol surface terminal groups formed in the worn region upon sliding in water without any significant rehybridization of carbon atoms from sp^3 to sp^2 bonding. The fraction of silanol surface terminal groups formed in the worn region upon sliding in water increases with the silicon content in Si-containing DLC, which is proposed to be the origin for the lower friction response achieved upon increasing the concentration of silicon

in the coating. This tribologically-induced change in surface termination did not lead to the adsorption of ATP upon incubation of tribostressed samples in ATP solutions for several hours. These findings provide guidance for the use of Si-containing DLC in biomedical applications that require the coating not only to be resistant to biomolecule adsorption in its as-deposited state, but also to have good tribological response in aqueous solution and to maintain good resistance to biomolecule adsorption after tribologically-induced variations in surface termination.

CRediT authorship contribution statement

Zixuan Li: Investigation, Formal analysis, Writing – original draft. **Jennings Z. Ye:** Investigation, Formal analysis, Writing – review & editing. **Jieming Yan:** Investigation, Formal analysis. **Nicolás Molina:** Investigation, Formal analysis. **Hsu-Ming Lien:** Investigation, Formal analysis. **Robert Chrostowksi:** Investigation, Formal analysis. **Cherno Jaye:** Investigation, Formal analysis, Writing – review & editing. **Daniel A. Fischer:** Investigation, Formal analysis, Writing – review & editing. **Jianliang Lin:** Investigation, Formal analysis. **Filippo Mangolini:** Conceptualization, Investigation, Formal analysis, Writing – original draft, Writing – review & editing.

Declaration of competing interest

The authors declare that they have no known competing financial interests or personal relationships that could have appeared to influence the work reported in this paper.

Acknowledgments

The material is based upon work supported by the Welch Foundation (Grant No. F-2002-20190330), the National Science Foundation Faculty Early Career Development Program (Grant No. 2042304), and the Taiho Kogyo Tribology Research Foundation (Grant No. 20A03). F.M. acknowledges support from the 2018 Ralph E. Powe Junior Faculty Enhancement Award sponsored by the Oak Ridge Associated Universities (ORAU), and from the Walker Department of Mechanical Engineering and the Texas Materials Institute at the University of Texas at Austin. Commercial names identified in this paper are for illustrative purpose and not intended to imply recommendation or endorsement by the National Institute of Standards and Technology.

Appendix A. Supplementary data

Supplementary data to this article can be found online at https://doi.org/10.1016/j.carbon.2022.07.043.

References

[1] E. Ebramzadeh, P.A. Campbell, K.M. Takamura, Z. Lu, S.N. Sangiorgio, J.J. Kalma, K.A. De Smet, H.C. Amstutz, Failure modes of 433 metal-on-metal hip implants: how, why, and wear, Orthop. Clin. N. Am. 42 (2) (2011) 241–250, ix.
[2] A. Grill, Diamond-like carbon coatings as biocompatible materials—an overview, Diam. Relat. Mater. 12 (2) (2003) 166–170.
[3] J. Robertson, Diamond-like amorphous carbon, Mater. Sci. Eng. R Rep. 37 (4–6) (2002) 129–281.
[4] A. Erdemir, C. Donnet, Tribology of diamond-like carbon films: recent progress and future prospects, J. Phys. Appl. Phys. 39 (18) (2006) R311.
[5] D.P. Dowling, P.V. Kola, K. Donnelly, T.C. Kelly, K. Brumitt, L. Lloyd, R. Eloy, M. Therin, N. Weill, Evaluation of diamond-like carbon-coated orthopaedic implants, Diam. Relat. Mater. 6 (2–4) (1997) 390–393.
[6] G. Gotzmann, J. Beckmann, C. Wetzel, B. Scholz, U. Herrmann, J. Neunzehn, Electron-beam modification of DLC coatings for biomedical applications, Surf. Coating. Technol. 311 (2017) 248–256.
[7] G. Dearnaley, J.H. Arps, Biomedical applications of diamond-like carbon (DLC) coatings: a review, Surf. Coating. Technol. 200 (7) (2005) 2518–2524.
[8] A. Hatem, J. Lin, R. Wei, R.D. Torres, C. Laurindo, P. Soares, Tribocorrosion behavior of DLC-coated Ti-6Al-4V alloy deposited by PIID and PEMS + PIID techniques for biomedical applications, Surf. Coating. Technol. 332 (2017) 223–232.
[9] M. Azzi, M. Paquette, J.A. Szpunar, J.E. Klemberg-Sapieha, L. Martinu, Tribocorrosion behaviour of DLC-coated 316L stainless steel, Wear 267 (5–8) (2009) 860–866.
[10] T.M. Manhabosco, I.L. Müller, Tribocorrosion of diamond-like carbon deposited on Ti6Al4V, Tribol. Lett. 33 (3) (2009) 193–197.
[11] R. Hauert, K. Thorwarth, G. Thorwarth, An overview on diamond-like carbon coatings in medical applications, Surf. Coating. Technol. 233 (2013) 119–130.
[12] A. Alanazi, C. Nojiri, T. Kido, T. Noguchi, Y. Ohgoe, T. Matsuda, K. Hirakuri, A. Funakubo, K. Sakai, Y. Fukui, Engineering analysis of diamond-like carbon coated polymeric materials for biomedical applications, Artif. Organs 24 (8) (2000) 624–627.
[13] L.A. Thomson, F.C. Law, N. Rushton, J. Franks, Biocompatibility of diamond-like carbon coating, Biomaterials 12 (1991) 37.
[14] S. Lousinian, S. Logothetidis, A. Laskarakis, M. Gioti, Haemocompatibility of amorphous hydrogenated carbon thin films, optical properties and adsorption mechanisms of blood plasma proteins, Biomol. Eng. 24 (1) (2007) 107–112.
[15] P. Yang, N. Huang, Y.X. Leng, J.Y. Chen, R.K.Y. Fu, S.C.H. Kwok, Y. Leng, P.K. Chu, Activation of platelets adhered on amorphous hydrogenated carbon (a-C:H) films synthesized by plasma immersion ion implantation-deposition (PIII-D), Biomaterials 24 (17) (2003) 2821–2829.
[16] S. Linder, W. Pinkowski, M. Aepfelbacher, Adhesion, cytoskeletal architecture and activation status of primary human macrophages on a diamond-like carbon coated surface, Biomaterials 23 (2002) 767.
[17] K. Gutensohn, C. Beythien, R. Koester, J. Bau, T. Fenner, P. Grewe, K. Padmanaban, P. Schaefer, P. Kuehnl, In vitro biocompatibility analyses of stents coated with diamond-like carbon by flow cytometry, cell growth assays and electron microscopy, Infusther. Transfusmed. 27 (2000) 200.
[18] F.Z. Cui, D.J. Li, A review of investigations on biocompatibility of diamond-like carbon and carbon nitride films, Surf. Coat. Technol. 131 (2000) 481.
[19] M. Allen, F. Law, N. Rushton, The effects of diamond-like carbon coatings on macrophages, fibroblasts and osteoblast-like cells in vitro, Clin. Mater. 17 (1994) 1.
[20] R.K. Roy, K.R. Lee, Biomedical applications of diamond-like carbon coatings: a review, J. Biomed. Mater. Res. B Appl. Biomater. 83 (1) (2007) 72–84.
[21] Y. Pauleau, Residual stresses in DLC films and adhesion to various substrates, in: C. Donnet, A. Erdemir (Eds.), Tribology of Diamond-Like Carbon Films: Fundamentals and Applications, Springer US, Boston, MA, 2008, pp. 102–136.
[22] P. Lemoine, J.P. Quinn, P.D. Maguire, J.A. McLaughlin, Mechanical characterisation and properties of DLC films, in: C. Donnet, A. Erdemir (Eds.), Tribology of Diamond-Like Carbon Films: Fundamentals and Applications, Springer US, Boston, MA, 2008, pp. 83–101.
[23] J. Fontaine, J.L. Loubet, T.L. Mogne, A. Grill, Superlow friction of diamond-like carbon films: a relation to viscoplastic properties, Tribol. Lett. 17 (4) (2004) 709–714.
[24] C. Donnet, A. Grill, Friction control of diamond-like carbon coatings, Surf. Coating. Technol. 94–95 (1997) 456–462.
[25] J.C. Sánchez-López, A. Fernández, Doping and alloying effects on DLC coatings, in: C. Donnet, A. Erdemir (Eds.), Tribology of Diamond-Like Carbon Films: Fundamentals and Applications, Springer US, Boston, MA, 2008, pp. 311–338.
[26] W.J. Yang, Y.-H. Choa, T. Sekino, K.B. Shim, K. Niihara, K.H. Auh, Thermal stability evaluation of diamond-like nanocomposite coatings, Thin Solid Films 434 (1,Äi2) (2003) 49–54.
[27] C. Jongwannasiri, X. Li, S. Watanabe, Improvement of thermal stability and tribological performance of diamond-like carbon composite thin films, Mater. Sci. Appl. 4 (2013) 630–636.
[28] T.W. Scharf, J.A. Ohlhausen, D.R. Tallant, S.V. Prasad, Mechanisms of friction in diamondlike nanocomposite coatings, J. Appl. Phys. 101 (6) (2007), 063521-11.
[29] D. Neerinck, P. Persoone, M. Sercu, A. Goel, D. Kester, D. Bray, Diamond-like nanocomposite coatings (a-C:H/a-Si:O) for tribological applications, Diam. Relat. Mater. 7 (2–5) (1998) 468–471.
[30] F. Mangolini, K.D. Koshigan, M.H. Van Benthem, J.A. Ohlhausen, J.B. McClimon, J. Hilbert, J. Fontaine, R.W. Carpick, How hydrogen and oxygen vapor affect the tribochemistry of silicon- and oxygen-containing hydrogenated amorphous carbon under low-friction conditions: a study combining X-ray absorption spectromicroscopy and data science methods, ACS Appl. Mater. Interfaces 13 (10) (2021) 12610–12621.
[31] K.D. Koshigan, F. Mangolini, J.B. McClimon, B. Vacher, S. Bec, R.W. Carpick, J. Fontaine, Understanding the hydrogen and oxygen gas pressure dependence of the tribological properties of silicon oxide–doped hydrogenated amorphous carbon coatings, Carbon 93 (2015) 851–860, 0.
[32] F. Mangolini, J. Hilbert, J.B. McClimon, J.R. Lukes, R.W. Carpick, Thermally induced structural evolution of silicon- and oxygen-containing hydrogenated amorphous carbon: a combined spectroscopic and molecular dynamics simulation investigation, Langmuir 34 (9) (2018) 2989–2995.
[33] J. Hilbert, F. Mangolini, J.B. McClimon, J.R. Lukes, R.W. Carpick, Si doping enhances the thermal stability of diamond-like carbon through reductions in carbon-carbon bond length disorder, Carbon 131 (2018) 72–78.
[34] R. Gilmore, R. Hauert, Control of the tribological moisture sensitivity of diamond-like carbon films by alloying with F, Ti or Si, Thin Solid Films 398–399 (2001) 199–204.
[35] D.C. Sutton, G. Limbert, D. Stewart, R.J.K. Wood, The friction of diamond-like carbon coatings in a water environment, Friction 1 (3) (2013) 210–221.
[36] H. Ronkainen, S. Varjus, K. Holmberg, Tribological performance of different DLC coatings in water-lubricated conditions, Wear 249 (3,Äì4) (2001) 267–271.
[37] N. Kato, H. Mori, N. Takahashi, Spectroscopic ellipsometry of silicon-containing diamond-like carbon (DLC-Si) films, Phys. Status Solidi 5 (5) (2008) 1117–1120.

[38] G. Zilibotti, S. Corni, M.C. Righi, Load-induced confinement activates diamond lubrication by water, Phys. Rev. Lett. 111 (14) (2013), 146101.
[39] S. Kajita, M.C. Righi, Insigths into the tribochemistry of silicon-doped carbon-based films by ab initio analysis of water–surface interactions, Tribol. Lett. 61 (2) (2016) 1–7.
[40] M.H. Ahmed, J.A. Byrne, J.A.D. McLaughlin, A. Elhissi, W. Ahmed, Comparison between FTIR and XPS characterization of amino acid glycine adsorption onto diamond-like carbon (DLC) and silicon doped DLC, Appl. Surf. Sci. 273 (2013) 507–514, 0.
[41] F. Mangolini, Reactivity of Environmentally Compatible Lubricant Additives: an in Situ and Ex Situ Investigation, Swiss Federal Institute of Technology (ETH), Doctoral Degree, 2011.
[42] F. Mangolini, A. Rossi, N.D. Spencer, Chemical reactivity of triphenyl phosphorothionate (TPPT) with iron: an ATR/FT-IR and XPS investigation, J. Phys. Chem. C 115 (4) (2011) 1339–1354.
[43] C.J. Powell, The physical basis for quantitative surface analysis by auger electron spectroscopy and X-ray photoelectron spectroscopy, in: N.S. McIntyre (Ed.), Quantitative Surface Analysis of Materials: American Society for Testing and Materials, 1978, pp. 5–30.
[44] S. Tanuma, Electron attenuation lengths, in: D. Briggs, J.T. Grant (Eds.), Surface Analysis by Auger and X-Ray Photoelectron Spectroscopy, IM Publications, Chichester (UK), 2003, pp. 259–294.
[45] A. Konicek, C. Jaye, M. Hamilton, W. Sawyer, D. Fischer, R. Carpick, Near-edge X-ray absorption fine structure imaging of spherical and flat counterfaces of ultrananocrystalline diamond tribological contacts: a correlation of surface chemistry and friction, Tribol. Lett. 44 (1) (2011) 99–106.
[46] F. Mangolini, J.B. McClimon, Near edge X-ray absorption fine structure spectroscopy: a powerful Tool for investigating the surface structure and chemistry of solid lubricants, in: M. Dienwiebel, M.I. De Barros Bouchet (Eds.), Advanced Analytical Methods in Tribology, Springer, 2018, pp. 63–106.
[47] F. Mangolini, J.B. McClimon, R.W. Carpick, Quantitative evaluation of the carbon hybridization state by near edge X-ray absorption fine structure spectroscopy, Anal. Chem. 88 (5) (2016) 2817–2824.
[48] F. Mangolini, Z. Li, M.A. Marcus, R. Schneider, M. Dienwiebel, Quantification of the carbon bonding state in amorphous carbon materials: a comparison between EELS and NEXAFS measurements, Carbon 173 (2021) 557–564.
[49] J. Stohr, NEXAFS Spectroscopy, Springer-Verlag, 1992.
[50] J.F. Moulder, W.F. Stickle, P.E. Sobol, K.D. Bomben, Handbook of X-Ray Photoelectron Spectroscopy, Perkin-Elmer Corporation, Physical Electronics Division, Eden Prairie, MN, USA, 1992.
[51] W. Hartung, A. Rossi, S. Lee, N. Spencer, Aqueous lubrication of SiC and Si3N4 ceramics aided by a brush-like copolymer additive, poly(l-lysine)-graft-poly (ethylene glycol), Tribol. Lett. 34 (3) (2009) 201–210.
[52] F. Mangolini, F. Rose, J. Hilbert, R.W. Carpick, Thermally induced evolution of hydrogenated amorphous carbon, Appl. Phys. Lett. 103 (16) (2013), 161605.
[53] G. Beamson, D. Briggs, High Resolution XPS of Organic Polymers: the Scienta ESCA300 Database, John Wiley & Sons, Chichester (UK), 1992.
[54] M.R. Alexander, R.D. Short, F.R. Jones, W. Michaeli, C.J. Blomfield, A study of HMDSO/O2 plasma deposits using a high-sensitivity and -energy resolution XPS instrument: curve fitting of the Si 2p core level, Appl. Surf. Sci. 137 (1,Äì4) (1999) 179–183.
[55] M.R. Alexander, R.D. Short, F.R. Jones, M. Stollenwerk, J. Zabold, W. Michaeli, An X-ray photoelectron spectroscopic investigation into the chemical structure of deposits formed from hexamethyldisiloxane/oxygen plasmas, J. Mater. Sci. 31 (7) (1996) 1879–1885.
[56] M. Yang, M.J. Marino, V.J. Bojan, O.L. Eryilmaz, A. Erdemir, S.H. Kim, Quantification of oxygenated species on a diamond-like carbon (DLC) surface, Appl. Surf. Sci. 257 (17) (2011) 7633–7638.
[57] S. Dreiner, M. Schürmann, C. Westphal, Investigation of the SiO2/Si(1 0 0) interface structure by means of angle-scanned photoelectron spectroscopy and diffraction, J. Electron. Spectrosc. Relat. Phenom. (2004) 79–84, 137–140(0).
[58] P.H.T. Ngamou, J.P. Overbeek, R. Kreiter, H.M. van Veen, J.F. Vente, I.M. Wienk, P.F. Cuperus, M. Creatore, Plasma-deposited hybrid silica membranes with a controlled retention of organic bridges, J. Mater. Chem. 1 (18) (2013) 5567–5576.
[59] M.P. Seah, S.J. Spencer, Ultrathin SiO2 on Si IV. Intensity measurement in XPS and deduced thickness linearity, Surf. Interface Anal. 35 (6) (2003) 515–524.
[60] N. Stojilovic, Why can't we see hydrogen in X-ray photoelectron spectroscopy? J. Chem. Educ. 89 (10) (2012) 1331–1332.
[61] A.C. Ferrari, J. Robertson, Interpretation of Raman spectra of disordered and amorphous carbon, Phys. Rev. B 61 (20) (2000) 14095–14107.
[62] C. Casiraghi, A.C. Ferrari, J. Robertson, Raman spectroscopy of hydrogenated amorphous carbons, Phys. Rev. B 72 (8) (2005), 085401.
[63] A.C. Ferrari, J. Robertson, Resonant Raman spectroscopy of disordered, amorphous, and diamondlike carbon, Phys. Rev. B 64 (7) (2001), 075414.
[64] F. Rose, N. Wang, R. Smith, Q.-F. Xiao, H. Inaba, T. Matsumura, Y. Saito, H. Matsumoto, Q. Dai, B. Marchon, F. Mangolini, R.W. Carpick, Complete characterization by Raman spectroscopy of the structural properties of thin hydrogenated diamond-like carbon films exposed to rapid thermal annealing, J. Appl. Phys. 116 (12) (2014), 123516.
[65] W.G. Cui, Q.B. Lai, L. Zhang, F.M. Wang, Quantitative measurements of sp3 content in DLC films with Raman spectroscopy, Surf. Coating. Technol. 205 (7) (2010) 1995–1999.
[66] W.-J. Wu, M.-H. Hon, Thermal stability of diamond-like carbon films with added silicon, Surf. Coating. Technol. 111 (2–3) (1999) 134–140.
[67] A.A. Ogwu, R.W. Lamberton, S. Morley, P. Maguire, J. McLaughlin, Characterisation of thermally annealed diamond like carbon (DLC) and silicon modified DLC films by Raman spectroscopy, Phys. B Condens. Matter 269 (3–4) (1999) 335–344.
[68] S.-E. Ong, S. Zhang, H. Du, D. Sun, Relationship between bonding structure and mechanical properties of amorphous carbon containing silicon, Diam. Relat. Mater. 16 (8) (2007) 1628–1635.
[69] H.S. Jung, H.H. Park, Determination of local bonding configuration and structural modification in amorphous carbon with silicon incorporation, Diam. Relat. Mater. 12 (8) (2003) 1373–1377.
[70] T.S. Santra, C.H. Liu, T.K. Bhattacharyya, P. Patel, T.K. Barik, Characterization of diamond-like nanocomposite thin films grown by plasma enhanced chemical vapor deposition, J. Appl. Phys. 107 (12) (2010) 124320–124329.
[71] K.-R. Lee, M.-G. Kim, S.-J. Cho, K. Yong Eun, T.-Y. Seong, Structural dependence of mechanical properties of Si incorporated diamond-like carbon films deposited by RF plasma-assisted chemical vapour deposition, Thin Solid Films 308-309 (1997) 263–267.
[72] N. Ohtake, M. Hiratsuka, K. Kanda, H. Akasaka, M. Tsujioka, K. Hirakuri, A. Hirata, T. Ohana, H. Inaba, M. Kano, H. Saitoh, Properties and classification of diamond-like carbon films, Materials 14 (2) (2021).
[73] G. Comelli, J. St$\sqrt{\partial}$hr, C.J. Robinson, W. Jark, Structural studies of argon-sputtered amorphous carbon films by means of extended x-ray-absorption fine structure, Phys. Rev. B 38 (11) (1988) 7511–7519.
[74] D.S. Grierson, A.V. Sumant, A.R. Konicek, T.A. Friedmann, J.P. Sullivan, R. W. Carpick, Thermal stability and rehybridization of carbon bonding in tetrahedral amorphous carbon, J. Appl. Phys. 107 (3) (2010), 033523-033525.
[75] F. Mangolini, J.B. McClimon, F. Rose, R.W. Carpick, Accounting for nanometer-thick adventitious carbon contamination in X-ray absorption spectra of carbon-based materials, Anal. Chem. 86 (24) (2014) 12258–12265.
[76] A.V. Sumant, P.U.P.A. Gilbert, D.S. Grierson, A.R. Konicek, M. Abrecht, J.E. Butler, T. Feygelson, S.S. Rotter, R.W. Carpick, Surface composition, bonding, and morphology in the nucleation and growth of ultra-thin, high quality nanocrystalline diamond films, Diam. Relat. Mater. 16 (4–7) (2007) 718–724.
[77] A. Wada, T. Ogaki, M. Niibe, M. Tagawa, H. Saitoh, K. Kanda, H. Ito, Local structural analysis of a-SiCx:H films formed by decomposition of tetramethylsilane in microwave discharge flow of Ar, Diam. Relat. Mater. 20 (3) (2011) 364–367.
[78] I. Ishii, A.P. Hitchcook, The oscillator strengths for C1s and O1s excitation of some saturated and unsaturated organic alcohols, acids and esters, J. Electron. Spectrosc. Relat. Phenom. 46 (1) (1988) 55–84.
[79] S. Osswald, G. Yushin, V. Mochalin, S.O. Kucheyev, Y. Gogotsi, Control of sp2/sp3 carbon ratio and surface chemistry of nanodiamond powders by selective oxidation in air, J. Am. Chem. Soc. 128 (35) (2006) 11635–11642.
[80] S.G. Urquhart, A.P. Hitchcock, R.D. Priester, E.G. Rightor, Analysis of polyurethanes using core excitation spectroscopy. Part II: inner shell spectra of ether, urea and carbamate model compounds, J. Polym. Sci. B Polym. Phys. 33 (11) (1995) 1603–1620.
[81] A.R. Konicek, D.S. Grierson, A.V. Sumant, T.A. Friedmann, J.P. Sullivan, P.U.P. A. Gilbert, W.G. Sawyer, R.W. Carpick, Influence of surface passivation on the friction and wear behavior of ultrananocrystalline diamond and tetrahedral amorphous carbon thin films, Phys. Rev. B 85 (15) (2012), 155448.
[82] B. Gilbert, B.H. Frazer, F. Naab, J. Fournelle, J.W. Valley, G. De Stasio, X-ray absorption spectroscopy of silicates for in situ, sub-micrometer mineral identification, Am. Mineral. 88 (5–6) (2003) 763–769.
[83] D.S. Grierson, A.V. Sumant, A.R. Konicek, M. Abrecht, J. Birrell, O. Auciello, J. A. Carlisle, T.W. Scharf, M.T. Dugger, P.U.P.A. Gilbert, R.W. Carpick, Tribochemistry and material transfer for the ultrananocrystalline diamond-silicon nitride interface revealed by x-ray photoelectron emission spectromicroscopy, J. Vac. Sci. Technol. B: Microelectron. Nanometer Struct. 25 (5) (2007) 1700–1705.
[84] B. Shi, Y.K. Shin, A.A. Hassanali, S.J. Singer, DNA binding to the silica surface, J. Phys. Chem. B 119 (34) (2015) 11030–11040.
[85] I. Sit, S. Sagisaka, V.H. Grassian, Nucleotide adsorption on iron(III) oxide nanoparticle surfaces: insights into nano-geo-bio interactions through vibrational spectroscopy, Langmuir 36 (51) (2020) 15501–15513.
[86] C.J. Brinker, Hydrolysis and condensation of silicates: effects on structure, J. Non-Cryst. Solids 100 (1–3) (1988) 31–50.